Volume 24, No 4 | International Journal of Radiation Research, October 2026

Relative peripheral retinal defocus patterns assessed by multispectral refractive topography and their association with myopia-related ocular parameters in early school-aged children

J. Wang[1], Z. Dou[2], X. Wang[3]

[1]*Department of Ophthalmology, The Fourth Affiliated Hospital, Zhejiang University School of Medicine, Yiwu, China*
[2]*Department of Respiratory and Critical Care Medicine, The Fourth Affiliated Hospital, Zhejiang University School of Medicine, Yiwu, China*
[3]*Department of Emergency Medicine, The Fourth Affiliated Hospital, Zhejiang University School of Medicine, Yiwu, China*

► ***Original article***

Corresponding author:
Jiani Wang, MM,
E-mail: *wangjiani@zju.edu.cn*

Received: June 2025
Final revised: June 2026
Accepted: June 2026

Int. J. Radiat. Res., October 2026; 24(4): 935-942

DOI: 10.61186/ijrr.24.4.2

Keywords: *Early school-aged children, myopia, relative peripheral retinal defocus, multispectral refractive topography, ocular biometry.*

ABSTRACT

Background: Relative peripheral retinal defocus has been implicated in refractive development, but multispectral refractive topography (MRT) patterns in early school-aged children remain incompletely characterized. This study evaluated MRT-derived relative peripheral retinal defocus patterns and their associations with myopia-related ocular parameters. ***Materials and Methods:*** This study included 115 children, aged 5-8 years, who underwent cycloplegic autorefraction, optical biometry, and MRT between July and November 2024. Right-eye data were analyzed. Spherical equivalent (SE), axial length (AL), mean keratometry (Km), and the axial length/corneal radius ratio (AL/CR) were calculated. Relative peripheral retinal defocus parameters were measured within a 53°retinal field and classified into volcanic mouth, hemiolateral upturned, saddle, and relatively flat patterns. Correlations and between-group differences were analyzed. ***Results:*** Diopter sphere (DS) was negatively correlated with total retinal defocus value (TRDV), 0-30°defocus (RDV-30), 0-45°defocus (RDV-45), 15-30°defocus (RDV-15-30), 30-45°defocus (RDV-30-45), and inferior defocus value (RDV-I) (all $P<0.05$). SE was negatively correlated with RDV-30, RDV-45, RDV-15-30, RDV-30-45, and RDV-I (all $P<0.05$). The hemiolateral upturned pattern was the most frequent pattern (31.30%), followed by the volcanic mouth (26.09%), saddle (22.61%), and relatively flat (20.00%) patterns. SE, DS, AL, AL/CR, and regional defocus parameters differed significantly among patterns ($P<0.05$). ***Conclusion:*** MRT-derived relative peripheral retinal defocus patterns were associated with refractive status and ocular biometry in early school-aged children. The volcanic mouth pattern was linked to a more myopic ocular profile, whereas the relatively flat pattern was linked to a more hyperopic profile.

INTRODUCTION

Myopia ranks among the foremost causes of visual impairment worldwide. In children, its prevalence has reached alarming levels, especially in East Asia [1]. The clinical burden of myopia extends beyond the need for optical correction because high myopia is associated with myopic maculopathy, retinal detachment, glaucoma, and other vision-threatening complications [2]. Beyond these ocular complications, the socioeconomic impact of myopia is considerable, encompassing increased healthcare expenditures, reduced quality of life, and impaired educational and occupational opportunities for affected individuals. The rising prevalence also places a growing strain on healthcare systems, particularly in regions where myopia has reached near-epidemic proportions. Increasing evidence suggests that refractive changes may begin before school age, and earlier onset is associated with a higher risk of high myopia later in life [3, 4]. Therefore, early school age (5-8 years) represents a critical window for identifying children at risk and implementing preventive strategies [5, 6]. During this period, the eye undergoes rapid growth and the emmetropization process is actively ongoing, making it particularly amenable to early interventions that could alter the natural course of refractive development.

Peripheral retinal defocus is considered one of the optical signals involved in ocular growth regulation and myopia development [7]. Accumulative evidence from animal and clinical studies demonstrates that relative peripheral hyperopic defocus may promote axial elongation, whereas relative peripheral myopic defocus may provide an inhibitory signal for eye growth [8]. However, peripheral defocus presents significant spatial asymmetry and regional heterogeneity, which cannot be fully characterized by

[Downloaded from ijrr.com on 2026-11-08]

[DOI: 10.61186/ijrr.24.4.2]

central axial refraction alone. Standard clinical assessments that rely solely on central refraction may therefore miss crucial information about an individual's risk profile for myopia development. Traditional peripheral refractometers can only measure defocus at limited meridians and cannot reflect the full-field spatial distribution of retinal defocus. Consequently, a comprehensive understanding of peripheral defocus patterns has remained elusive, limiting the clinical utility of this optical parameter in routine practice.

Multispectral refractive topography (MRT) is a non-invasive method that evaluates retinal refractive status within a 53-degree field centered on the fovea and generates a topographic map of peripheral defocus [9, 10]. Previous studies have demonstrated the feasibility and repeatability of MRT for assessing peripheral refraction in children and other age groups [11]. Recent cross-sectional studies have found that MRT-derived peripheral defocus parameters differ significantly among children with different refractive states, and are correlated with axial length growth [12, 13]. Despite these advances, the distribution of MRT-derived relative peripheral retinal defocus patterns in early school-aged children remains insufficiently described. At this age, refractive development is often in transition from physiological hyperopia toward emmetropia or myopia [14].

Clarifying the spatial patterns of peripheral retinal defocus and their associations with SE, AL, and other ocular biometric parameters may help improve early myopia risk stratification. The innovative aspect of this study lies in the fact that it fills the gap of MRT-based peripheral defocus phenotype data in this critical refractive development period, and reveals the association between different defocus spatial patterns and myopia-related ocular biometric parameters. These findings may provide a new optical phenotype indicator for early identification of myopia risk, and offer fundamental data for subsequent longitudinal studies on myopia progression. Accordingly, this study used MRT to classify relative peripheral retinal defocus patterns in children aged 5-8 years and to examine their associations between topographic patterns and standard biometric parameters. Concurrently, the rich patient data gathered in the present work will be repurposed to create an AI-powered instructional framework. This framework is specifically intended to bolster autonomous learning competencies among medical trainees.

MATERIALS AND METHODS

Study design and participants

The study included 115 early school-aged children (115 right eyes) who underwent refractive and ocular examinations between July and November 2024. Only the right eye of each participant was selected for analysis to avoid inter-eye correlation. The cohort included 62 boys and 53 girls. The median age was 8 years, with an interquartile interval of 7-8 years. Inclusion criteria: (1) age 5-8 years; (2) ability to cooperate with ophthalmic examinations and MRT testing; (3) best-corrected visual acuity >=0.8; (4) no abnormality on anterior segment or fundus examination; and (5) intraocular pressure values within the between 10 and 21 mmHg. Exclusion criteria: (1) organic ocular disorders, including strabismus, amblyopia, keratitis, glaucoma, or congenital cataract; (2) previous ocular trauma or ophthalmic surgery; (3) systemic diseases potentially affecting visual development, including autoimmune disease, diabetes, or neurologic disease; and (4) missing or poor-quality data. This study was approved by the Institutional Review Board of our hospital, (Approval No. K2025283).

Routine ocular measurements

A non-contact tonometer (NT-510; NIDEK, Tokyo, Japan) served to measure IOP, and participants with abnormal intraocular pressure (outside 10–21 mmHg) were excluded. For cycloplegic refraction, compound tropicamide eye drops (Handan Kangye Pharmaceutical Co., Ltd., Hebei, China) were administered four times every 5-minute. Administration continued until the pupil reached >6 mm with no observable light response, which indicated full cycloplegia. Autorefraction was then performed using an automated refractometer (KR-800; TOPCON, Tokyo, Japan). Each eye was measured 3 consecutive times. Diopter sphere (DS), diopter cylinder (DC), and cylinder axis (AX) were recorded. Spherical equivalent (SE = DS + 1/2 DC) and classified as myopia (SE <= -0.50 D), emmetropia (-0.50 D < SE < +0.50 D), hyperopia (SE >= +0.50 D) [15]. Axial length and corneal keratometry were measured using an optical biometer (LS900; Haag-Streit AG, Koeniz, Switzerland). Flat keratometry (K1), steep keratometry (K2), mean keratometry (Km = [K1 + K2]/2), and AL/CR (CR = 337.5/Km) were calculated.

Detection and classification of relative peripheral retinal defocus

Multispectral refractive topography quantified relative peripheral retinal defocus. (MSIC2000, Thondar Technology Co., Ltd, Shenzhen, China). The instrument acquires multispectral retinal images through 12 wavelengths, and calculates relative defocus values of different retinal regions based on chromatic aberration principle. The following parameters were obtained: total retinal defocus value (TRDV), 0-15° defocus (RDV-15), 0-30° defocus (RDV-30), 0-45° defocus (RDV-45), 15-30° defocus (RDV-15-30), 30-45° defocus (RDV-30-45), 45-53°

[Downloaded from ijrr.com on 2026-11-08]

[DOI: 10.61186/ijrr.24.4.2]

defocus (RDV-45-53), superior defocus (RDV-S), inferior defocus (RDV-I), nasal defocus (RDV-N), and temporal defocus (RDV-T). A positive RDV value indicates relative peripheral hyperopic defocus, meaning that peripheral images fall posterior to the retina. A negative value indicates relative peripheral myopic defocus, meaning that peripheral images focus anterior to the retina.

During MRT examination, each participant was seated with the chin and forehead positioned on the instrument supports and was instructed to fixate on the built-in red target. The examiner adjusted alignment and focus before image acquisition. Each eye was measured three consecutive times, and the mean value from measurements with confidence >=90% was used for analysis. All examinations were performed by the same experienced ophthalmologist who had completed standardized MRT operation training to ensure consistency. The spatial distribution and topographic parameters of relative peripheral retinal defocus are illustrated in figure 1.

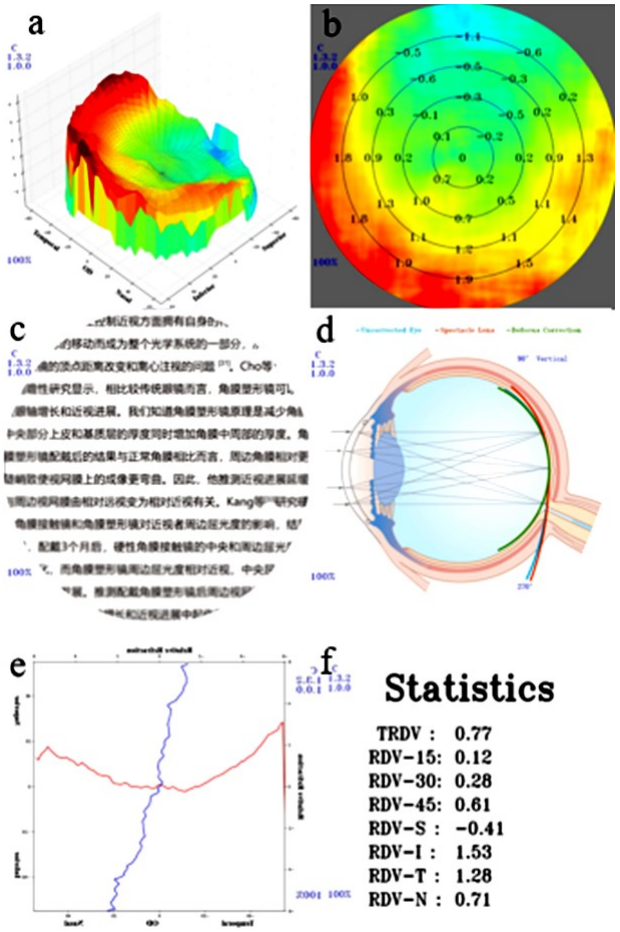


Figure 1. Representative multispectral refractive topography (MRT) report. **(a)** Stereogram. **(b)** Point map. **(c)** Visual effect diagram. **(d)** Defocus schematic. **(e)** Defocus curve. **(f)** Topographic parameters.

Based on MRT topographic morphology, relative peripheral retinal defocus was classified into four patterns: volcanic mouth, hemiolateral upturned, saddle, and relatively flat. All MRT images were independently assessed by two experienced ophthalmic examiners who were fully masked to participants' demographic information, refractive status and other ocular parameters. Any inconsistent results between the two examiners were resolved via mutual discussion to reach a final agreement. The volcanic mouth pattern was characterized by circumferential peripheral hyperopic defocus greater than the central region. The hemiolateral upturned pattern showed markedly increased hyperopic defocus in one hemiretinal region. The saddle pattern showed increased hyperopic defocus in two opposing retinal regions. The relatively flat pattern showed low hyperopic defocus across retinal regions with an overall flat distribution (figure 2).

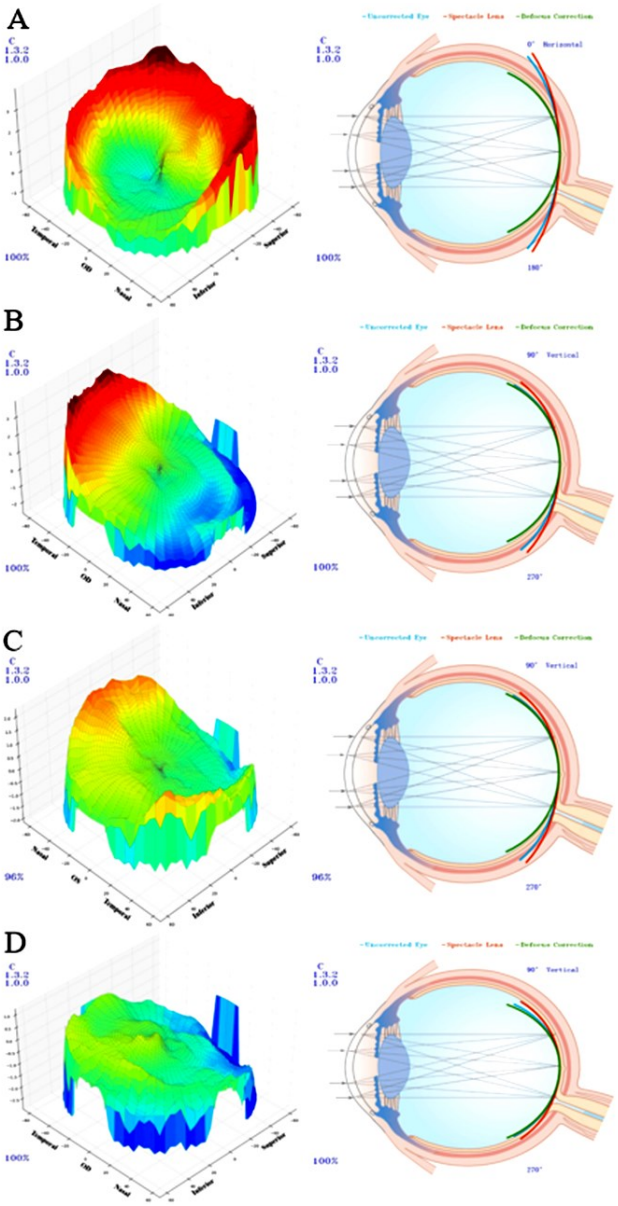


Figure 2. Schematic diagram of four relative peripheral retinal defocus patterns. **(A)** Volcanic mouth pattern. **(B)** Hemiolateral upturned pattern. **(C)** Saddle pattern. **(D)** Relatively flat pattern.

[Downloaded from ijrr.com on 2026-11-08]

[DOI: 10.61186/ijrr.24.4.2]

Statistical analysis

Data were analyzed with SPSS 22.0. Normality was checked via Shapiro–Wilk test. Normally and non-normally distributed continuous data are reported as (`x±s) and median (IQR), respectively. Correlations employed Pearson or Spearman tests. MRT pattern comparisons used one-way ANOVA with Bonferroni post-hoc. Categorical data were compared by c^2. Significance was set at two-sided $P<0.05$.

RESULTS

Distribution of refractive status, ocular biometric parameters, and peripheral defocus parameters

Under cycloplegic conditions, the right eye showed myopia in 67 participants (58.26%), emmetropia in 20 participants (17.39%), and hyperopia in 28 participants (24.35%). The median SE was -0.63 D (interquartile range: -1.25 to 0.38 D), with a range from -5.25 to 1.75 D. AL ranged from 21.07 to 25.68 mm, with a mean of 23.62 +/- 0.85 mm. The mean keratometry values were 42.75 +/- 1.31 D for K1, 43.93 +/- 1.48 D for K2, and 43.34 +/- 1.36 D for Km. The mean AL/CR was 3.03 +/- 0.09. Regarding defocus variables, TRDV ranged from -0.85 to 1.00 D, with a mean of 0.19 +/- 0.35 D. The detailed regional and quadrant-specific defocus values are summarized in the corresponding tables and figures.

Correlation between refractive parameters and relative peripheral retinal defocus

Pearson and Spearman correlation analyses showed that DS was negatively correlated with TRDV, RDV-30, 45, 15-30, 30-45, and RDV-I ($P<0.05$). SE was negatively correlated with RDV-30, 45, 15-30, 30-45, and RDV-I ($P<0.05$). DC and AX were not significantly correlated with the relative peripheral retinal defocus parameters ($P>0.05$) (table 1).

Table 1. Correlation analysis between refractive parameters and regional peripheral retinal defocus.

parameter	DS（D）	DC（D）	AX（°）	SE（D）
TRDV	-0.207[a*]	0.005[b]	-0.031[b]	-0.173[b]
RDV-15	-0.072[b]	0.096[b]	-0.053[b]	-0.053[b]
RDV-30	-0.229[b*]	0.023[b]	0.004[b]	-0.223[b*]
RDV-45	-0.253[a*]	0.003[b]	-0.006[b]	-0.212[b*]
RDV-15-30	-0.246[b*]	0.015[b]	0.013[b]	-0.242[b*]
RDV-30-45	-0.238[a*]	-0.01[b]	-0.013[b]	-0.204[b*]
RDV-45-53	-0.098[a]	0.022[b]	-0.073[b]	-0.068[b]
RDV-S	-0.055[b]	0.119[b]	-0.135[b]	-0.045[b]
RDV-I	-0.190[a*]	-0.055[b]	0.006[b]	-0.201[b*]
RDV-T	-0.150[a]	0.149[b]	-0.112[b]	-0.128[b]
RDV-N	-0.167[a]	-0.146[b]	0.109[b]	-0.154[b]

*P<0.05. a Pearson analysis; b Spearman analysis.Diopter sphere: DS; Diopter cylinder: DC; Cylinder axis: AX; Spherical equivalent: SE; Total retinal defocus value: TRDV; 0-15°defocus: RDV-15; 0-30°defocus: RDV -30; 0-45°defocus: RDV-45; 15-30°defocus: RDV-15-30; 30-45°defocus: RDV-30-45; 45-53°defocus: RDV-45-53; Superior: S; Inferior: I; Temporal: T; Nasal: N.

Among the 115 early school-aged children, the hemiolateral upturned pattern was the most common MRT classification, observed in 36 participants (31.30%). The volcanic mouth pattern was observed in 30 participants (26.09%), the saddle pattern in 26 participants (22.61%), and the relatively flat pattern in 23 participants (20.00%). Myopia was most frequent in the volcanic mouth pattern (80.00%) and hemiolateral upturned pattern (75.00%), whereas hyperopia was most frequent in the relatively flat pattern (69.56%). The distribution of refractive status differed significantly across MRT patterns (chi-square = 41.00, $P<0.001$; calculated from the counts in table 2).

Table 2. Distribution of myopia, emmetropia, and hyperopia across different peripheral retinal defocus patterns.

Defocus pattern	Number	Percentage
Volcanic mouth type (n=30)	myopia (n=24)	80.00%
	emmetropia (n=4)	13.33%
	hyperopia (n=2)	6.67%
Hemiolateral upturned type (n=36)	myopia (n=27)	75.00%
	emmetropia (n=5)	13.89%
	hyperopia (n=4)	11.11%
Saddle type (n=26)	myopia (n=14)	53.84%
	emmetropia (n=6)	23.08%
	hyperopia (n=6)	23.08%
Relatively flat type (n=23)	myopia (n=2)	8.70%
	emmetropia (n=5)	21.74%
	hyperopia (n=16)	69.56%

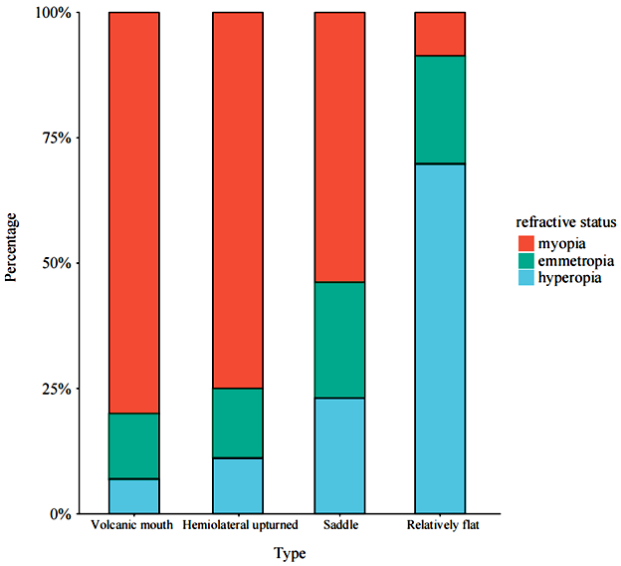


Figure 3. Distribution of refractive status across different relative peripheral retinal defocus patterns in early school-aged children.

Comparison of ocular biometric parameters among MRT classifications

Overall comparisons showed significant differences in SE, DS, AL, AL/CR among the four MRT patterns (all $P<0.001$). In pairwise comparisons, the hemiolateral upturned pattern had a shorter AL than the volcanic mouth pattern ($P<0.05$). The saddle and relatively flat patterns had higher SE and DS values than the volcanic mouth pattern ($P<0.05$). The relatively flat pattern had lower AL and AL/CR values

[Downloaded from ijrr.com on 2026-11-08]
[DOI: 10.61186/ijrr.24.4.2]

than the volcanic mouth pattern (P<0.05), higher SE and DS values and a lower AL/CR than the hemiolateral upturned pattern (P<0.05), and higher SE and DS values than the saddle pattern (P<0.05). (table 3).

Table 3. Comparison of ocular biometric parameters among different relative peripheral retinal defocus patterns.

Defocus pattern	SE(D)	DS(D)	DC(D)	Km(D)	AL(mm)	AL/CR
Volcanic mouth type (n=30)	-1.58± 1.37	-1.31± 1.28	-0.53± 0.62	43.05± 1.50	24.11± 0.87	3.07± 0.09
Hemiolateral upturned type (n=36)	-0.87± 0.90	-0.74± 0.88	-0.26± 0.32	43.72± 1.28	23.55± 0.73[a]	3.05± 0.07
Saddle type (n=26)	-0.38± 0.94[a]	-0.20± 0.90[a]	-0.36± 0.33	43.26± 1.27	23.58± 0.77	3.02± 0.08
Relatively flat type (n=23)	0.70± 0.96[abc]	0.94± 1.08[abc]	-0.47± 0.68	43.25± 1.36	23.11± 0.80[a]	2.96± 0.07[ab]
F value	21.068	21.773	1.914	1.457	7.226	9.838
P value	<0.001	<0.001	0.131	0.230	<0.001	<0.001

Compared with the volcanic mouth pattern, aP<0.05; compared with the hemiolateral upturned pattern, bP<0.05; compared with the saddle pattern, cP<0.05. Spherical equivalent: SE; Diopter sphere: DS; Diopter cylinder: DC; Mean keratometry: Km; Cylinder axis: AX; Axial length/corneal radius ratio: AL/CR.

Box-plot analysis further showed that the relatively flat pattern had the highest SE and DS values and the lowest AL and AL/CR values, whereas the volcanic mouth pattern showed the lowest SE and DS values and the highest AL and AL/CR values (figure 4). These findings suggest that MRT classification is associated with refractive and biometric profiles.

Comparison of peripheral retinal defocus parameters among MRT classifications

Peripheral retinal defocus parameters differed significantly across the four MRT patterns, including TRDV, RDV-15, 30, 45, 15-30, 30-45, 45-53, S, I, T, N (P<0.05). Compared with the saddle pattern, the relatively flat pattern had lower TRDV, RDV-30, 45, 15-30, 30-45, 45-53, S, T, N (P<0.05). The volcanic mouth pattern had higher TRDV, RDV-45, 30-45, 45-53, I (P<0.05). The hemiolateral upturned pattern had lower RDV-45-53, N but higher RDV-I (P<0.05). (table 4).

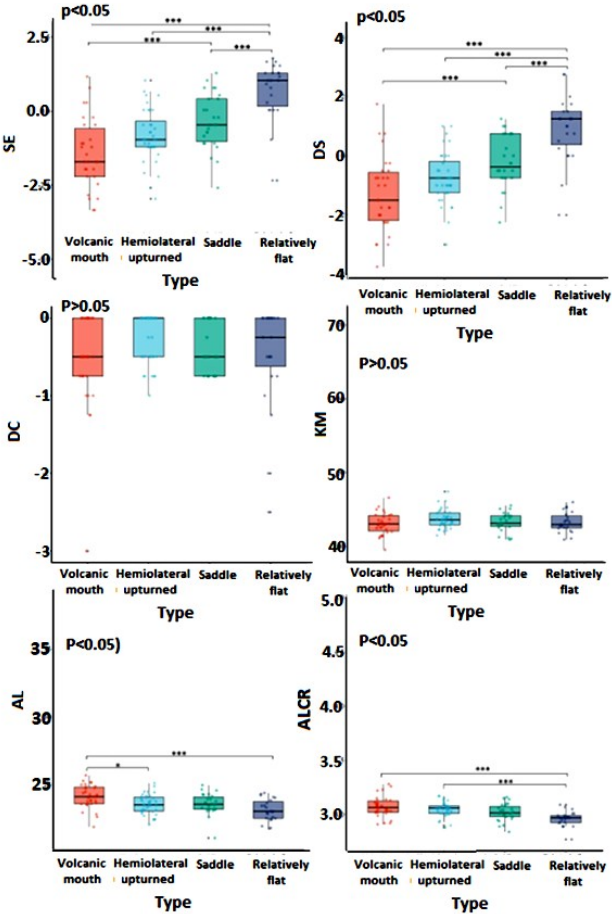


Figure 4. Box-plot distribution of ocular biometric parameters across different relative peripheral retinal defocus patterns in early school-aged children. *P<0.05; ***P<0. 001.delete overlap data with table.

Table 4. Comparison of peripheral retinal defocus parameters among different relative peripheral retinal defocus. patterns.

Defocus pattern	Saddle type (n=26)	Relatively flat type (n=23)	Volcanic mouth type (n=30)	Hemiolateral upturned type (n=36)	*F* value	*P* value
TRDV (D)	0.25±0.25	-0.13±0.30[a]	0.51±0.25[ab]	0.08±0.28[bc]	27.138	<0.001
RDV-15 (D)	0.01±0.07	-0.03±0.09	0.04±0.07[b]	0.02±0.07	3.787	<0.05
RDV-30 (D)	0.00±0.13	-0.17±0.22[a]	0.11±0.17[b]	0.01±0.18[b]	10.794	<0.001
RDV-45 (D)	0.15±0.18	-0.16±0.27[a]	0.38±0.22[ab]	0.06±0.26[bc]	23.218	<0.001
RDV-15-30 (D)	-0.00±0.16	-0.21±0.26[a]	0.14±0.20[b]	0.01±0.23[b]	11.436	<0.001
RDV-30-45 (D)	0.27±0.26	-0.15±0.35[a]	0.59±0.29[ab]	0.09±0.32[bc]	28.002	<0.001
RDV-45-53 (D)	0.61±0.54	-0.05±0.47[a]	0.97±0.44[ab]	0.16±0.42[ac]	26.773	<0.001
RDV-S (D)	-0.38±0.43	-0.77±0.50[a]	-0.28±0.60[b]	-0.94±0.40[ac]	12.960	<0.001
RDV-I (D)	0.47±0.43	0.26±0.28	0.99±0.31[ab]	0.82±0.46[ab]	19.531	<0.001
RDV-T (D)	0.69±0.49	0.36±0.30[a]	0.90±0.36[b]	0.67±0.45[b]	7.664	<0.001
RDV-N (D)	0.29±0.44	-0.34±0.51[a]	0.50±0.47[b]	-0.18±0.41[ac]	21.083	<0.001

Compared with the saddle pattern, aP<0.05; compared with the relatively flat pattern, bP<0.05; compared with the volcanic mouth pattern, cP<0.05. Total retinal defocus value: TRDV; 0-15°defocus: RDV-15; 0-30°defocus: RDV-30; 0-45°defocus: RDV-45; 15-30°defocus: RDV-15-30; 30-45° defocus: RDV-30-45; 45-53°defocus: RDV-45-53; Superior: S; Inferior: I; Temporal: T; Nasal: N

[Downloaded from ijrr.com on 2026-11-08]

[DOI: 10.61186/ijrr.24.4.2]

DISCUSSION

China faces one of the most severe myopia epidemics globally. Domestic epidemiological data indicate that the prevalence of myopia among children and adolescents is 36.6%, and that of high myopia is 5.3% [16]. Children aged 5–8 years stay within an essential window of visual maturation, during which the refractive system gradually completes the emmetropization process alongside somatic growth. Critical ocular biometric indicators experience continuous dynamic changes during this developmental stage, deviations in these processes form the essential pathological underpinning for the initiation and advancement of myopia [17]. Peripheral retinal defocusing is the core mechanism that drives the abnormal growth of the eye axis, and it is also a key factor to mediate the development and progression of myopia. Multispectral refractive topography (MRT) is a new non-invasive technology to detect the defocus around the retina. This technology can collect fundus images and rely on algorithms to complete the calculation of relevant parameters by evaluating fine-grained feature variations across multi-wavelength fundus imaging data [18]. Compared with the traditional axial multi-point measurement method, a novel multispectral-based refractor offers the advantages of rapid measurement and good repeatability. Additionally, by capturing refractive data at multiple eccentricities across four quadrants, this technology enables the generation of a comprehensive spatial distribution map of peripheral defocus [19]. This study uses MRT technology to type the peripheral defocusing characteristics of the retinal in early school-age children, systematically analyze the MRT distribution characteristics of periretinal defocusing, deeply explore the correlation between periretinal defocus and refractive parameters, reveal the significance of myopia risk of different MRT types, and accurately screen for children's myopia. Investigation and individualized prevention and control provide a new theoretical basis.

The observed negative correlations between DS/SE and peripheral defocus parameters are consistent with previous evidence suggesting that relative peripheral hyperopic defocus may be related to axial elongation and myopia development [7, 18, 20-22]. In this cohort, RDV-I showed a significant association with central refractive status, suggesting that inferior retinal defocus may be particularly relevant during early school age. This regional association may reflect asymmetry in visual input, near-work posture, and local retinal signaling. Furthermore, several lines of evidence support this regional specificity. In terms of mechanism, the reduction of SE will further amplify the farsighted defocus signal of the peripheral retina and strengthen the driving effect on the growth of the eye axis. The comprehensive characteristics of SE enable it to more sensitively capture the change between the central refraction and the peripheral defocus [7]. Prior studies have confirmed that different retinal regions contribute asymmetrically to refractive development, with the inferior retina playing a particularly prominent role [23]. This regional specificity may be related to visual behavior patterns in young children. Early school-aged children aged 5-8 years are in a stage of gradually increasing near-work activity; a large amount of daily near-gaze exposure may cause the inferior retina to be chronically subjected to hyperopic defocus from near targets, thereby becoming a key driver of abnormal axial growth [24]. Animal models have verified that local retinal defocus can induce corresponding regional changes in ocular shape, providing a biological basis for this quadrant-specific effect [8]. In addition, correlation studies in adults have shown that DS is negatively correlated not only with RDV-I but also with RDV-S and RDV-T [17]. The absence of such correlations in the present study may be related to the fact that the ocular shape in school-aged children is still undergoing rapid remodeling; the superior and temporal retinal defocus distributions have not yet formed a stable pattern and exhibit large inter-individual variability, whereas in other age groups the peripheral defocus profile has matured and the associated signals are more stable. Nevertheless, because this was a cross-sectional study, the results should be interpreted as associations rather than evidence of a causal mechanism.

The four MRT patterns appeared to represent different spatial configurations of peripheral defocus. The volcanic mouth pattern showed broadly increased peripheral hyperopic defocus and was associated with a more myopic ocular profile, including lower SE, longer AL, and higher AL/CR. In contrast, the relatively flat pattern showed lower peripheral hyperopic defocus and was associated with a more hyperopic profile. These findings support the potential value of MRT pattern classification for describing refractive development phenotypes in young children. However, the term 'protective effect' should be avoided unless supported by longitudinal follow-up data. Each MRT type corresponds to a different degree and spatial configuration of peripheral defocus, and the defocus signal regulates scleral remodeling to influence axial growth, thereby leading to differences in SE, DS, AL, and AL/CR [19]. Research suggests that the spatial configuration of defocus can regulate scleral remodeling and axial elongation through visual signaling pathways [25]. For instance, full-circumferential high defocus (such as the crater type) may have a stronger driving effect on axial growth by widely activating visual signaling pathways, whereas unilateral defocus predominance (such as the hemiolateral upturned type) may alter

[Downloaded from ijrr.com on 2026-11-08]

[DOI: 10.61186/ijrr.24.4.2]

the biomechanical balance of the eyeball and drive axial shift in a specific direction [26]. This association between spatial configuration and biometric parameters also confirms the internal mechanism underlying the significant negative correlation between RDV-I and DS/SE.

Clinically, MRT may provide complementary information beyond central refraction and axial length by visualizing the spatial distribution of peripheral defocus. Such information may help identify children with different myopia-related ocular profiles and may inform individualized myopia management strategies. In current clinical practice, optical interventions for myopia management - including orthokeratology, peripheral defocus-correcting spectacles, and multifocal soft contact lenses - all operate on the fundamental mechanism of mitigating or reversing peripheral retinal hyperopic defocus [27]. The present study demonstrated that children with higher baseline peripheral hyperopic defocus, particularly those with elevated hyperopic defocus in the mid-peripheral region (30°–45°), as well as those exhibiting volcanic mouth or hemiolateral upturned defocus patterns, carry significantly elevated risk for myopia onset and progression. These subgroups may represent optimal candidates for peripheral defocus-modifying interventions, and early intervention in these populations might more effectively enhance myopia control outcomes. Whether children with more pronounced baseline hyperopic defocus demonstrate superior clinical responses to these interventions remains to be validated through large-scale and long-duration controlled clinical trials, which would provide a basis for optimizing clinical protocols. At present, MRT morphological pattern recognition faces prominent challenges in ophthalmology teaching. The diverse topographic manifestations and subjective criteria for manual classification increase the learning difficulty for novice practitioners, while traditional offline teaching is limited by insufficient standard cases and inconsistent assessment standards, resulting in low training efficiency. Therefore, it is urgent to develop AI-assisted autonomous learning systems to standardize the teaching and training of MRT interpretation. The standardized MRT retinal topographic images, clear classification labels of four defocus patterns, and matched clinical ocular parameter data obtained in this study can serve as high-quality annotated teaching datasets. These resources can effectively support the development, training and optimization of AI-based MRT teaching platforms, help standardize the interpretation criteria of peripheral retinal defocus patterns, and improve the overall proficiency of ophthalmic trainees in mastering MRT technology.

Several limitations warrant consideration. First, the retrospective cross-sectional methodology does not allow for causal interpretations or projections of subsequent myopia progression. Second, the cohort was relatively limited in size and drawn from a single institution. Third, other factors, such as near work, outdoor time, parental myopia, and prior optical correction, were not fully controlled. Fourth, morphological classification of MRT patterns requires further validation, ideally using masked graders, interobserver agreement analysis, objective clustering methods, and longitudinal datasets.

CONCLUSIONS

In early school-aged children, DS and SE were negatively associated with total and regional relative peripheral retinal defocus parameters, especially in the mid-peripheral and inferior retinal regions. In the context of this developmental period, hyperopic defocus within these specific regions emerges as a pivotal factor driving both the initiation and advancement of myopia, and the parameters associated with this defocus phenomenon show promise as early biomarkers for identifying myopia susceptibility. MRT-derived relative peripheral retinal defocus patterns were associated with distinct refractive and ocular biometric profiles. In our current investigation, the MRT type of retinal relative peripheral defocus was predominantly the hemiolateral upturned type. The volcanic mouth pattern was linked to a more myopic profile, whereas the relatively flat pattern was linked to a more hyperopic profile. These findings suggest that MRT may be useful for characterizing myopia-related ocular phenotypes in early school-aged children. In summary, MRT examination serves as an effective tool for early screening and risk stratification of myopia in young school-aged children, providing a new basis for individualized prevention and control strategies in this population. Future prospective longitudinal studies - which we plan to conduct - are warranted to ascertain whether these MRT patterns can forecast myopia onset or progression and to validate their role in clinical risk stratification.

Acknowledgments: We would like to thank all the medical staff in the Department of Ophthalmology at the Fourth Affiliated Hospital of Zhejiang University School of Medicine for their strong support and assistance during data collection and outpatient coordination. We also thank all the children who participated in this study and their parents for their understanding and cooperation.

Conflict of interest: All authors declare no conflicts of interest related to the content of this study.

Funding: This study was supported by a general research grant from the Zhejiang Provincial Department of Education (Grant No.: Y202558313).

Ethical consideration: This study strictly adheres to the ethical guidelines of the Declaration of Helsinki,

[Downloaded from ijrr.com on 2026-11-08]

[DOI: 10.61186/ijrr.24.4.2]

and the study protocol has been approved by the Ethics Committee of the Fourth Affiliated Hospital of Zhejiang University School of Medicine (Approval No.: K2025283). Following review by the Ethics Committee, approval was granted to collect data for this retrospective study, and informed consent was waived.

***Project funding support*:** General Scientific Research Project of Zhejiang Provincial Department of Education (Y202558313): A Comparative Study on the Use of Generative AI in Self-Directed Learning Among Chinese and Foreign Medical Students

***Authors' contribution*:** J.W.: Responsible for the research conception and design, ethics application, data collection and analysis, and manuscript drafting and revision; as the corresponding author, she was responsible for manuscript submission and communication. Z.D.: Participated in data collection and organization, as well as statistical analysis. X.W.: Assisted with data entry, statistical analysis, and literature search.

REFERENCES

1. Liang J, Pu Y, Chen J, *et al.* (2025) Global prevalence, trend and projection of myopia in children and adolescents from 1990 to 2050: a comprehensive systematic review and meta-analysis. *Br J Ophthalmol,* ***109****(3): 362-371*.
2. Du Y, Meng J, He W, *et al.* (2024) Complications of high myopia: An update from clinical manifestations to underlying mechanisms. *Adv Ophthalmol Pract Res,* ***4****(3): 156-163*.
3. Liu WC, Guo H, Lam CSY, *et al.* (2025) Axial length growth trajectories in children transitioning to myopia. *Am J Ophthalmol,* ***279****(1): 223-233*.
4. Hu Y, Ding X, Guo X, *et al.* (2020) Association of age at myopia onset with risk of high myopia in adulthood in a 12-year follow-up of a Chinese cohort. *JAMA Ophthalmol,* ***138****(11): 1129-1134*.
5. Liu L, Li R, Huang D, *et al.* (2021) Prediction of premyopia and myopia in Chinese preschool children: a longitudinal cohort. *BMC Ophthalmol,* ***21****(1): 283*.
6. Bullimore MA and Brennan NA (2023) Myopia: An ounce of prevention is worth a pound of cure. *Ophthalmic Physiol Opt,* ***43*** *(1): 116-121*.
7. Erdinest N, London N, Lavy I, *et al.* (2023) Peripheral defocus as it relates to myopia progression: A mini-review. *Taiwan J Ophthalmol,* ***13****(3): 285-292*.
8. Swiatczak B, Scholl HPN, Schaeffel F (2024) Retinal "sweet spot" for myopia treatment. *Scientific Reports,* ***14****(1): 26773*.
9. Ni NJ, Ma FY, Wu XM, *et al.* (2021) Novel application of multispectral refraction topography in the observation of myopic control effect by orthokeratology lens in adolescents. *World J Clin Cases,* ***9****(30): 8985-8998*.
10. Li T, Jiang B, Zhou X (2025) Assessment of relative peripheral refraction in children with low myopia and pre-myopia using multispectral refraction topography. *Sci Rep,* ***15****(1): 21361*.
11. Xiaoli L, Xiangyue Z, Lihua L, *et al.* (2022) Comparative study of relative peripheral refraction in children with different degrees of myopia. *Front Med (Lausanne),* ***9****: 800653*.
12. Song Z, Wang Y, Li Y, *et al.* (2026) Peripheral retinal defocus in children and adolescents with different refractive statuses and its relationship with refractive parameters. *BMC Ophthalmol,* ***26****(1): 215*.
13. Xie F, Mao X, Jiang M, *et al.* (2025) Alterations in peripheral refraction are most significant just before the onset of myopia: evidence from multispectral refraction topography. *Ophthalmol Ther,* ***14****(9): 2125-2139*.
14. Pu J, Fang Y, Zhou Z, *et al.* (2025) The hyperopia reserve in 3- to 6-years-old preschool children in North China: the Beijing hyperopia reserve research. *BMC Ophthalmol,* ***25****(1): 175*.
15. Peñaloza-Barbosa MI, Martinez-Perez C, Andreu-Vázquez C, *et al.* (2025) Spherical equivalent percentile curves in a Portuguese school-aged population. *J Clin Med,* ***14****(20): 7262*.
16. Pan W, Saw SM, Wong TY, *et al.* (2025) Prevalence and temporal trends in myopia and high myopia children in China: a systematic review and meta-analysis with projections from 2020 to 2050. *Lancet Reg Health West Pac,* ***55****(1): 101484*.
17. Troilo D, Smith EL 3rd, Nickla DL, *et al.* (2019) IMI - Report on experimental models of emmetropization and myopia. *Invest Ophthalmol Vis Sci,* ***60****(3): M31-M88*.
18. Bao T, Qin L, Hou G, *et al.* (2024) Association between peripheral retinal defocus and myopia by multispectral refraction topography in Chinese children. *Clin Ophthalmol,* ***18****: 517-523*.
19. Lu W, Ji R, Ding W, *et al.* (2021) Agreement and repeatability of central and peripheral refraction by one novel multispectral-based refractor. *Front Med (Lausanne),* ***8****(1): 777685*.
20. Du Y, Zhang M, Zhou Y, *et al.* (2024) Observations on relative peripheral refraction in Chinese adults with myopia based on a novel application of multispectral refraction topography. *Sci Rep,* ***14****(1): 25854*.
21. Wu DW, Yang ZY, Nie Y, *et al.* (2024) Refraction difference value variations in children and adolescents with different refractive errors. Int J Ophthalmol, **17**(12): 2236-2242.
22. Zhao Q, Wang Y, Liang T, *et al.* (2024) Characteristics of peripheral retinal refraction and its role in children with different refractive states. *J Ophthalmol,* ***2024****: 7712516*.
23. QU S, SONG F, LI Y, *et al.* (2025) Analysis of the effects of corneal and lens characteristics on peripheral defocus of the retina and its relationship with myopia. *Sci Rep,* ***15****(1): 22102*.
24. Choi KY, Mok AY, Do CW, *et al.* (2020) The diversified defocus profile of the near-work environment and myopia development. *Ophthalmic Physiol Opt,* ***40****(4): 463-471*.
25. Brown DM, Mazade R, Clarkson-Townsend D, *et al.* (2022) Candidate pathways for retina to scleral signaling in refractive eye growth. *Exp Eye Res,* ***219****(1): 109071*.
26. Zheng XH, Shi HL, You JX, *et al.* (2024) A study on the distribution characteristics of peripheral retinal defocus in children and adolescents. *Zhonghua Yan Ke Za Zhi,* ***60****(4):337-342*.
27. Lanca C, Pang CP, Grzybowski A (2023) Effectiveness of myopia control interventions: A systematic review of 12 randomized control trials published between 2019 and 2021. *Front Public Health,* ***11****(1): 1125000*.

[Downloaded from ijrr.com on 2026-11-08]

[DOI: 10.61186/ijrr.24.4.2]